Available online at www.sciencedirect.com

ScienceDirect

journal homepage: www.elsevier.com/locate/he

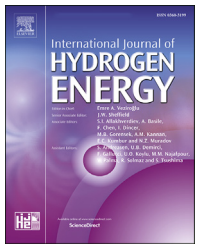

Catalytic behaviour of transition metal carbides of group 5 in the methanol steam reforming

Arturo Pajares [a,b,1], *Pilar Ramírez de la Piscina* [a], *Narcís Homs* [a,b,*]

[a] *Department de Química Inorgànica i Orgànica, Secció de Química Inorgànica & Institut de Nanociència i Nanotecnología (IN2UB), Universitat de Barcelona, Martí i Franquès 1-11, 08028 Barcelona, Spain*
[b] *Catalonia Institute for Energy Research (IREC), Jardins de les Dones de Negre 1, 08930 Barcelona, Spain*

HIGHLIGHTS

- Group 5 transition metal carbides as catalysts in the methanol steam reforming.
- Methanol steam reforming over VC, NbC and TaC polycrystalline catalysts.
- H_2+CH_4 mixtures are obtained under MSR over VC catalyst.
- HCHO is obtained under MSR over NbC and TaC catalysts.

ARTICLE INFO

Article history:
Received 28 October 2022
Received in revised form
31 May 2023
Accepted 2 June 2023
Available online 21 June 2023

Keywords:
MSR
VC
NbC
TaC
H_2+CH_4 mixtures production
HCHO production

ABSTRACT

Transition metal carbides of group 5 (G5TMC=VC, NbC and TaC) with similar crystallite sizes were prepared by a sol-gel route. The catalysts were characterized and studied in the methanol steam reforming (MSR) reaction in the temperature range of 573–723 K at atmospheric pressure and using a stoichiometric CH_3OH/H_2O = 1/1 mole ratio mixture. Under the MSR reaction conditions used, the route of methanol transformation depends on the G5TMC used as catalyst. The catalytic behaviour of VC differs from that of NbC and TaC, which in turn show a similar behaviour. Over VC, methanol is mainly converted to a mixture of H_2+CH_4, whereas over NbC and TaC the major product obtained is HCHO, formed from the dehydrogenation of methanol.

* *Corresponding author*. Department de Química Inorgànica i Orgànica, secció de Química Inorgànica & Institut de Nanociència i Nanotecnología (IN2UB), Universitat de Barcelona, Martí i Franquès 1-11, 08028 Barcelona, Spain.
E-mail address: narcis.homs@qi.ub.edu (N. Homs).
[1] Present address: Sustainable Materials Management, Flemish Institute for Technological Research (VITO NV), Boeretang 200, 2400 Mol, Belgium.

https://doi.org/10.1016/j.ijhydene.2023.06.017

Introduction

Nowadays, unlike oil or natural gas, H_2 transport still presents important drawbacks for its large use as clean energy carrier [1]. In this context, liquid carriers are considered one of the potential routes to facilitate the convenient transport of H_2 [2]. In particular, liquid alcohols are considered interesting H_2 storage chemical systems and useful H_2 carriers. Methanol is the simplest alcohol and possesses several advantages for H_2 transport and delivery: it has a high hydrogen to carbon ratio, it can be produced from captured CO_2, and it has been reported as the cheapest option among different liquid organic hydrogen carriers [3].

These aspects make methanol an attractive route for both the chemical recycling of CO_2, including that biomass-derived, and the renewable H_2 storage and transport. Steam reforming-based processes of renewable methanol could be an alternative to the use of methane, to bring, where needed, not only H_2, but also other gaseous C-containing products of potential interest in the actual energy context. For instance, among others, syngas ($CO + H_2$) for further applications, or (H_2+CH_4) mixtures for its direct injection into the natural gas network distribution.

Despite methanol steam reforming (MSR) is an endothermic reaction (eq. (1)), the required temperature can be significantly lower than that necessary for the steam reforming of CH_4, if appropriate catalysts are used. In addition, the absence of C–C bonds can facilitate its reforming at lower temperature when compared to other higher alcohols.

$$CH_3OH + H_2O \rightarrow CO_2 + 3H_2 \quad \Delta H^0_{298} = 49.7 \text{ kJ mol}^{-1} \qquad \text{(eq. 1)}$$

Thus, the development of different catalytic systems effective for the MSR process could enlarge the knowledge and possibilities of this route in the basis of the above indicated interests.

Transition metal carbides (TMC) have gained much attention since Levy and Boudart reported that they have "platinum-like behaviour" as catalysts for certain reactions [4]. Following this idea, we have studied different TMCs as catalysts for the CO_2 reduction through the reverse water gas shift reaction as well as co-catalysts of photoactive materials [5–10].

To our knowledge, polycrystalline (hcp-Mo_2C), metal-modified molybdenum carbide and supported Mo_2C catalysts have been reported so far in the MSR reaction [11–15]. Considering this background, in this work we present for the first time, the study of the catalytic behaviour of polycrystalline TMC of group 5 (G5TMC=VC, NbC, and TaC) under stoichiometric MSR reaction conditions.

Experimental

Catalyst preparation

G5TMC catalysts (VC, NbC and TaC) with a similar crystallite size were prepared on the basis of a sol-gel method reported for the preparation of V_xC using 4,5-dicyanoimidazole as carbon precursor [6]. For this, specific conditions of precursors' ratio (VO(isopropoxide)$_2$, $NbCl_5$ or $TaCl_5$/4,5-dicyanoimidazole) and treatment temperature were used. For VC, 4.04 g of VO(isopropoxide)$_3$ (Alfa Aesar, 96%) were dissolved into 15 mL of ethanol (HPLC grade, 99.9%, Scharlau). Next, 1.95 g of 4,5-dicyanoimidazole (Manchester Organics, 96%) were added to the alcoholic solution with continuous stirring until forming a viscous solution [6]. A similar procedure was used for the preparation of NbC and TaC, but using the corresponding chlorides. 2.60 g of $NbCl_5$ (Alfa Aesar, 99%) and 2.32 g of 4,5-dicyanoimidazole were used in the case of NbC; 1.86 g of $TaCl_5$ (Alfa Aesar, 99.8%) and 1.89 g of 4,5-dicyanoimidazole were used for the TaC preparation; due to the poor solubility of $TaCl_5$ in ethanol, methanol (HPLC grade, 99.98%, Scharlau) was used for preparing the initial solution of $TaCl_5$. In all cases, the preparation was performed under Ar flow to avoid hydrolysis of the metal precursors. Afterward, the obtained viscous solutions were placed in a tubular furnace for thermal treatment under Ar (5 h, 2.5 K min^{-1}) up to 1373 K for VC and NbC, and up to 1423 K for TaC.

Catalyst characterization

Inductively-coupled plasma atomic emission spectrometry (ICP-AES) was used to determine the chemical composition of the catalysts. The ICP-AES measurements were carried out using a Perkin Elmer Optima 3200RL apparatus. Nitrogen adsorption-desorption isotherms were performed at 77 K, using a Micromeritics Tristar II 3020 instrument. Before the measurements, catalysts were degassed at 525 K for 5 h under N_2. The surface area (S_{BET}) was determined from the B.E.T. model and the pore size distribution was determined by applying the BHJ method. The catalysts were analysed by X-ray diffraction (XRD) with a PANalytical X'Pert PRO MPD Alpha1 powder diffractometer, using a Cu Kα radiation source (λ = 1.5406 Å). The crystallite size was calculated using the Debye-Scherrer equation. X-ray photoelectron spectroscopy (XPS) analysis was carried out in a Perkin Elmer PHI-5500 Multitechnique System, Physical Electronics. All spectra were collected using an Al X-ray source (hυ = 1486.6 eV and 350 W). Before XPS measurements, the C 1s BE of adventitious carbon at 284.8 eV was determined in the same equipment and conditions using Au as reference. Transmission electron microscopy and high resolution (TEM-HRTEM) images were collected employing a JEOL J2010 F microscope operated up to 200 kV. H_2-Temperature programmed reduction (H_2-TPR) experiments were performed in a Micromeritics Autochem II 2920 equipped with a thermal conductivity detector (TCD). Samples (about 100 mg) were pretreated at 363 K under He for 1 h and then exposed to an H_2/Ar (12% v/v) flow, later the temperature was increased up to 1073 K at 10 K min^{-1}. Raman spectroscopy analysis was performed in a Jobin-Yvon LabRam HR 800 instrument, with an optical Olympus BXFM microscope, with a 532 nm laser and a CCD detector. The laser power was restricted to 1.25 mW to avoid major laser-heating effects during spectra acquisition. Thermal gravimetric analysis (TGA/DSC) were carried out using a SenSysevo (Setaram) equipment coupled to a mass spectrometer (Pfeiffer Vacuum Omnistar). About 30 mg of the samples were placed in an alumina cell and heated under O_2/Ar (10% v/v) (10 mL/min) from room temperature to 1023 K (10 K min^{-1}). CO_2 was continuously monitored in the effluent.

Catalytic tests

The MSR reactions were performed in a Microactivity Reference (MA0571) unit (PID Eng&Tech) equipped with a GILSON 307 5SC HPLC pump. The stoichiometric reactant mixture, $CH_3OH/H_2O = 1$ (mol/mol), was injected at constant flow and atmospheric pressure, pre-heated at 473 K and mixed with N_2 (>99.999%), which was added to reach a gas hourly space velocity (GHSV) of 2500 h^{-1}. The gaseous mixture $CH_3OH/H_2O/N_2 = 1/1/1.2$ (molar ratio), was flowed through the catalyst at atmospheric pressure. In all cases, 300 mg of catalyst diluted with SiC, were placed in a tubular reactor, being the catalytic bed of 1 mL. Catalytic tests were carried out at 573, 623, 673 and 723 K, increasing the temperature from 573 K to 723 K. The first analysis at a given temperature was performed after 30 min of stabilization, and the temperature was kept for 1.5 h. The catalytic results at every temperature were determined by the average of at least three measurements. In order to evaluate the stability of the catalysts, all of them were kept at the highest reaction temperature (723 K) for 20 h.

Separate experiments varying the contact time were carried out with two representative catalysts (VC and NbC), by increasing N_2 flow, using $CH_3OH/H_2O/N_2 = 1/1/5.5$ and $CH_3OH/H_2O/N_2 = 1/1/8$ mixtures, resulting GHSV of 6000 and 8000 h^{-1}, respectively. For these experiments, fresh VC or NbC were studied first at 6000 h^{-1} (T = 598 and 623 K) and then at 8000 h^{-1} (T = 598 and 623 K), using an experimental procedure similar to that described above.

A liquid-gas separator fitted with a level sensor, working at 277 K, allowed the condensation of vapours. The total gaseous flow was measured at the outlet of the system, and analysed online employing a Varian 4900 micro-GC equipped with three channels with thermal conductivity detectors and M5A (Ar carrier), PPQ (He carrier), and 5CB (He carrier) columns.

The CH_3OH conversion (X_{CH_3OH}) was calculated as

$$X_{CH_3OH}(\%) = \frac{\sum a_i.(\eta_i)_{outlet}}{(\eta_{CH_3OH})_{inlet}} \cdot 100$$

The selectivity to C-containing compounds (S_i) is obtained as:

$$S_i(\%) = \frac{a_i.(\eta_i)_{outlet}}{\sum a_i.(\eta_i)_{outlet}} \cdot 100$$

Where a_i is the number of carbon atoms per molecule of the i product (CH_4, CO, CO_2, HCHO, C_2H_4, and C_2H_6). η_i is the number of moles of the i product (CH_4, CO, CO_2, HCHO, C_2H_4, and C_2H_6). η_{CH_3OH} is the number of moles of methanol in the reactants.

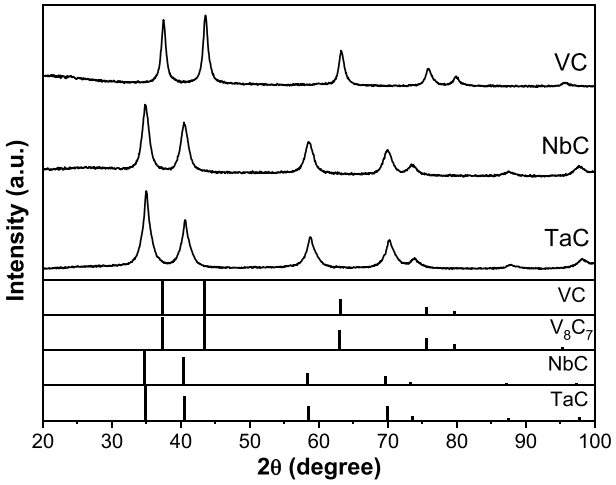

Fig. 1 – XRD patterns of G5TMC catalysts.

Results and discussion

Fig. 1 shows the XRD pattern of G5TMC catalysts. For NbC and TaC, the presence of carbide cubic phases is clearly determined (JCPDS 38–1364 and 35–0801, respectively). For VC, the presence of V_8C_7 (JCPDS 35–0786) can be deduced; however, the simultaneous presence of stoichiometric cubic VC (JCPDS 01-073-0476) cannot be ruled out (Fig. 1) [6].

In all cases, small crystallite sizes in the 9–11 nm range are determined from XRD analysis (Table 1). XRD peaks corresponding to crystalline oxides were not found in any case.

The Raman spectra of samples are shown in Fig. 2. No bands in the range 100–1000 cm^{-1} attributed to metal oxides (VO_x, NbO_x and TaO_x) can be observed. The bands around 1350 and 1600 cm^{-1} are due to residual carbon in the samples from the preparation step. G and D components and the corresponding G/D area ratios determined after a proper analysis [16] are shown in Table 1.

All catalysts are mesoporous materials with B.E.T. areas in the 220–290 $m^2\ g^{-1}$ range (Table 1).

HRTEM confirmed the presence of cubic VC and/or V_8C_7, NbC, and TaC (Figs. 3–5). The mean particle size determined by TEM was 11.6, 10.0 and 9.5 nm for VC, NbC, and TaC samples, respectively. These values agree very well with the crystallite sizes determined from XRD analysis (Table 1). For NbC and TaC, a small number of particles with larger sizes, 35–50 and 18–26 nm, respectively, can be observed (see histograms in Figs. 4 and 5).

Fig. 6 shows the H_2-TPR profiles of G5TMC samples; the H_2-consumptions were very small (0.06–0.45 mmol H_2/g_{cat}). The

Table 1 – Crystallite size, S_{BET} area, pore diameter and G/D area ratio (Raman) of fresh and used G5TMC catalysts.

Catalyst	Crystallite size (nm)	S_{BET} ($m^2\ g^{-1}$)		Pore size (nm)		G/D	
		Fresh	Used	Fresh	Used	Fresh	Used
VC	11	271	<10	7	35	0.22	0.29
NbC	9	290	110	2	3	0.19	0.24
TaC	9	220	<10	2	40	0.12	0.16

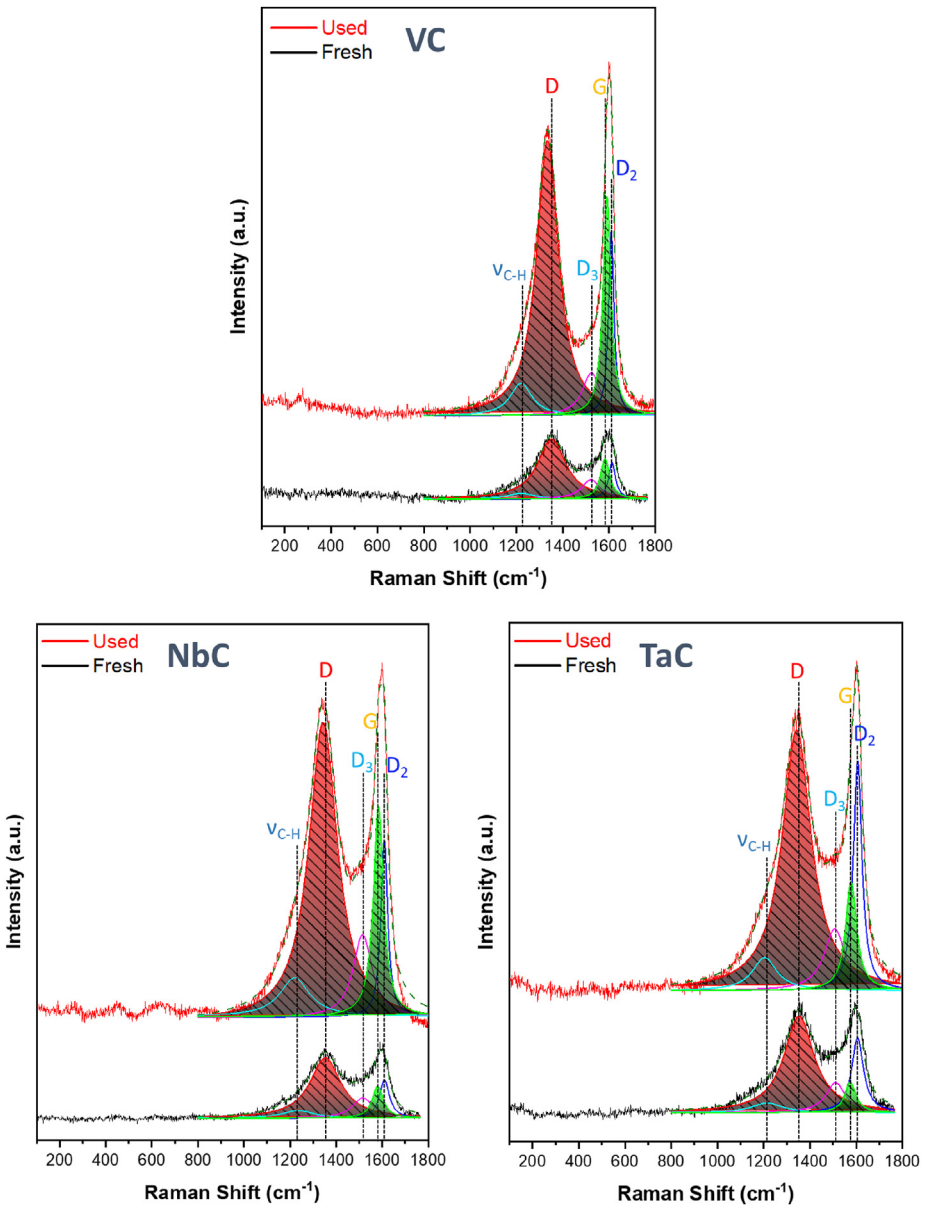

Fig. 2 – Raman spectra of fresh and used G5TMC catalysts in MSR (573–723 K, and 20 h at 723 K). Reaction conditions: $CH_3OH/H_2O/N_2$ = 1/1/1.2, P = 0.1 MPa, GHSV = 2500 h^{-1}.

consumption at about 498 K in VC sample can be related with the reduction of oxy-carbide species; the reduction of amorphous V_2O_5 takes place at ~852 K and that of crystalline V_2O_5 at higher temperatures [6,17,18]. For NbC and TaC samples, the very small H_2-consumption at about 630 K (Fig. 6), could be associated with niobium and tantalum oxy-carbide reduction. Nb_2O_5 and Ta_2O_5 reductions cannot be observed in this range of temperature because they take place at higher temperatures (>1173 K) [19–21]. Oxy-carbide species were likely formed when G5TMC were exposed to air after the preparation [5,6,8].

The G5TMC catalysts were also analysed by XPS. The C 1s spectra of samples are shown in Fig. 7. In all cases, a C 1s component centred at 283.0–283.2 eV assigned to carbide phase (VC, NbC, and TaC) is found [6,22,23]. The component at 284.8 eV is referred to C–C bond corresponding to residual and adventitious carbon, and those at higher BE are assigned to species with C–H, C–O, C=O, and/or C–O=O bonds [24–27]. Fig. 8 shows the V 2p, Nb 3d, and Ta 4f spectra corresponding to VC, NbC and TaC samples, respectively. In all cases, the component at the lowest BE, V $2p_{3/2}$ at 513.6 eV, Nb $3d_{5/2}$ at 204.1 eV, and Ta $4f_{7/2}$ at 23.8 eV, is attributed to the corresponding carbide species. The components at higher BEs, can be assigned to the presence of different surface V- [6,28,29], Nb- [22,30] and Ta- [23,31] oxy-carbide and oxide species.

The catalytic behaviour of G5TMC was studied under the MSR reaction conditions stated above. Fig. 9 displays the methanol conversion values as a function of temperature. As expected, in all cases, the MeOH conversion increased with the temperature increase up to 723 K. Fig. 9 also shows the product distribution for all G5TMC. In all cases, H_2, CH_4, CO, CO_2, HCHO, C_2H_4, and C_2H_6 were detected. However, over the

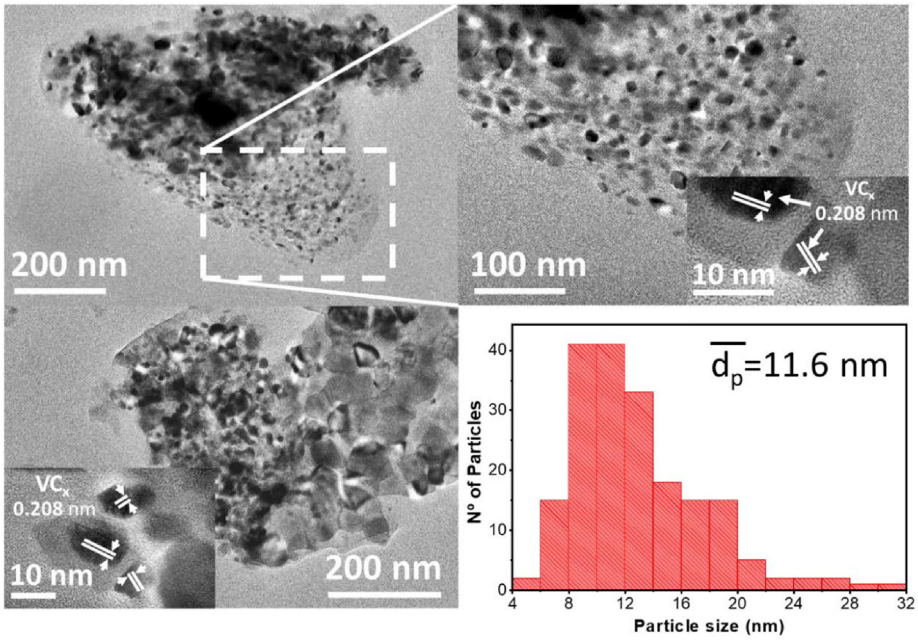

Fig. 3 – TEM, HRTEM (inset) images and particle size distribution of VC. d-spacing of 0.208 nm can be assigned to VC<100> or V_8C_7<200> planes.

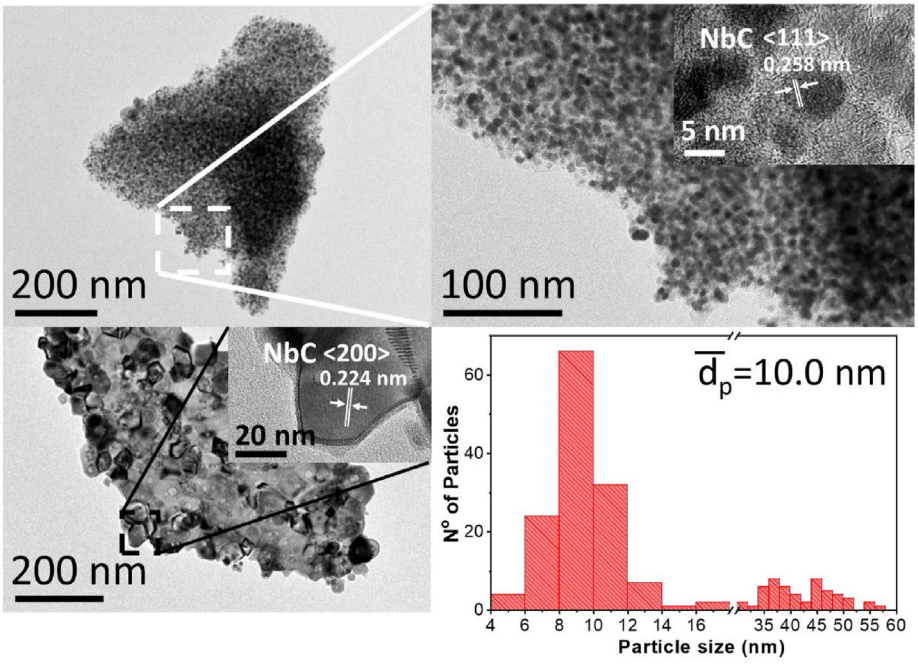

Fig. 4 – TEM, HRTEM (inset) images and particle size distribution of NbC.

different G5TMC, the catalytic transformation of methanol showed significant differences.

Over VC, in the overall temperature range, CH_4 and H_2 were the main products. At 573 K, similar production of CH_4 and H_2 was obtained (about 40% molar concentration each one). At this temperature, the molar concentration of CO and CO_2, was about 10% each one. At the highest temperature (723 K), an increase in the production of CH_4 and a decrease on that of H_2 could be noted, being the molar concentrations 57% and 23%, respectively. Over VC, the results indicate that under the reactions conditions used, the steam reforming process does not proceed in a large extension.

The CH_4 formation might be associated with the methanol decomposition, which could result in CH_4 and an adsorbed O on the surface (eq. (2)) [11,32–37], the latter could form surface oxy-carbide species. The oxy-carbide species subsequently could react with H_2 to recover the corresponding metal carbide producing H_2O.

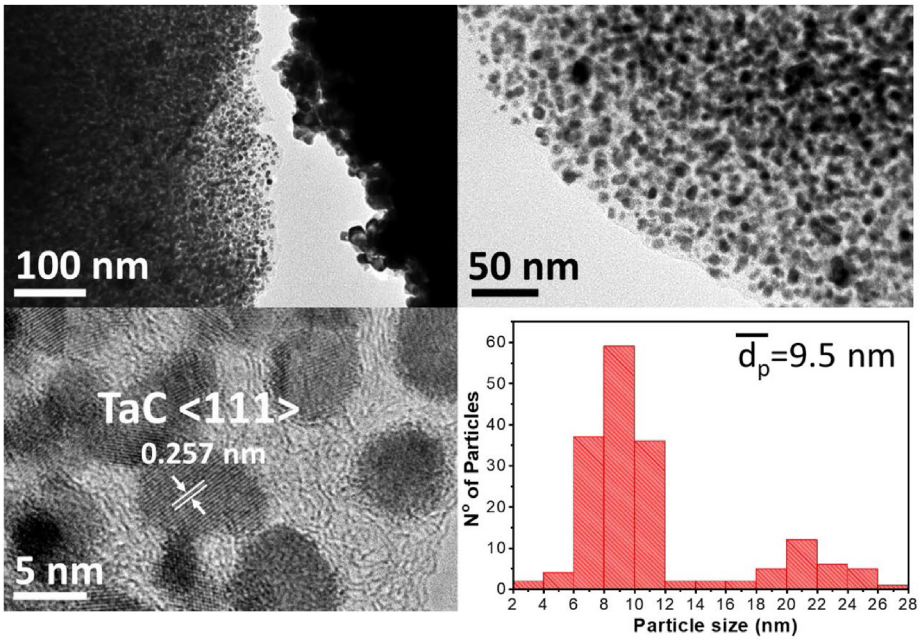

Fig. 5 – TEM, HRTEM images and particle size distribution of TaC.

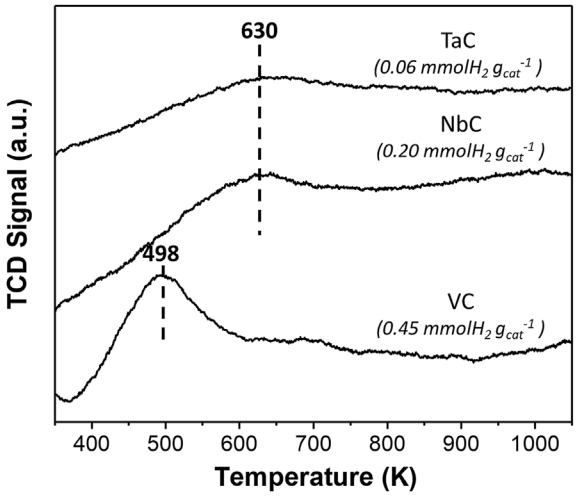

Fig. 6 – H_2-TPR profiles of G5TMC catalysts.

$$CH_3OH_{(ad)} \rightarrow CH_{4(g)} + O_{(ad)} \quad \text{(eq. 2)}$$

Studies of methanol decomposition over VC single crystals have shown that VC could break C–O instead of C–H bonds of methoxy intermediate species, leading to CH_4 production at ~500 K; this is possibly associated with the presence of defect sites (C vacancies) [38,39]. In fact, high selectivity to CH_4 is observed when methanol decomposition is carried out over carbide-modified metallic single crystals C/V (110) [38]. The presence of C vacancies has been also proposed as active centres for methanol activation on Mo_2C systems [14]. A similar process could take place over the VC catalyst under the MSR conditions used in this work. It is necessary to recall that the VC catalyst studied in this work contains defective V_8C_7 phases. However, depending on the temperature range considered, methanation reactions cannot be ruled out for CH_4 formation (eqs. (3) and (4)).

$$CO_{2(g)} + 4H_{2(g)} \rightarrow CH_{4(g)} + 2H_2O_{(g)} \quad \text{(eq. 3)}$$

$$CO_{(g)} + 3H_{2(g)} \rightarrow CH_{4(g)} + H_2O_{(g)} \quad \text{(eq. 4)}$$

Moreover, at low temperatures it could be necessary to take into account also the contribution of the WGS equilibrium (eq. (5)).

$$CO_{(g)} + H_2O_{(g)} \leftrightarrows CO_{2(g)} + H_{2(g)} \quad \text{(eq. 5)}$$

As a result, over the VC catalyst, mainly a H_2+CH_4 mixture is produced with $(H_2+CH_4)_{produced}/CH_3OH_{converted}$ (mol/mol) ratios higher than 0.78.

On the other hand, over NbC and TaC catalysts, the methanol transformation under the reaction conditions used, results in the main production of HCHO; being CH_4 and H_2 the other major products observed. At the lowest temperature, 573 K, mostly HCHO and H_2 were found; the HCHO selectivity referred to C-containing products obtained is about 95% for both NbC and TaC. For both catalysts, the HCHO selectivity decreases and that of CH_4 increases with the increasing of temperature. The CO and CO_2 molar concentrations were always well below 10%. These results point that over NbC and TaC catalysts, under the reactions conditions used, the reforming reaction neither takes place in an appreciable extension. The dehydrogenation of methanol to formaldehyde seems to be the main reaction pathway over NbC and TaC catalysts (eq. (6)).

$$CH_3OH_{(g)} \rightarrow HCHO_{(g)} + H_{2(g)} \quad \text{(eq. 6)}$$

On both samples, the scission of C–H in CH_3O species would be more favoured than C–O bond cleavage. The presence of CH_3O groups has been observed on NbC single crystals

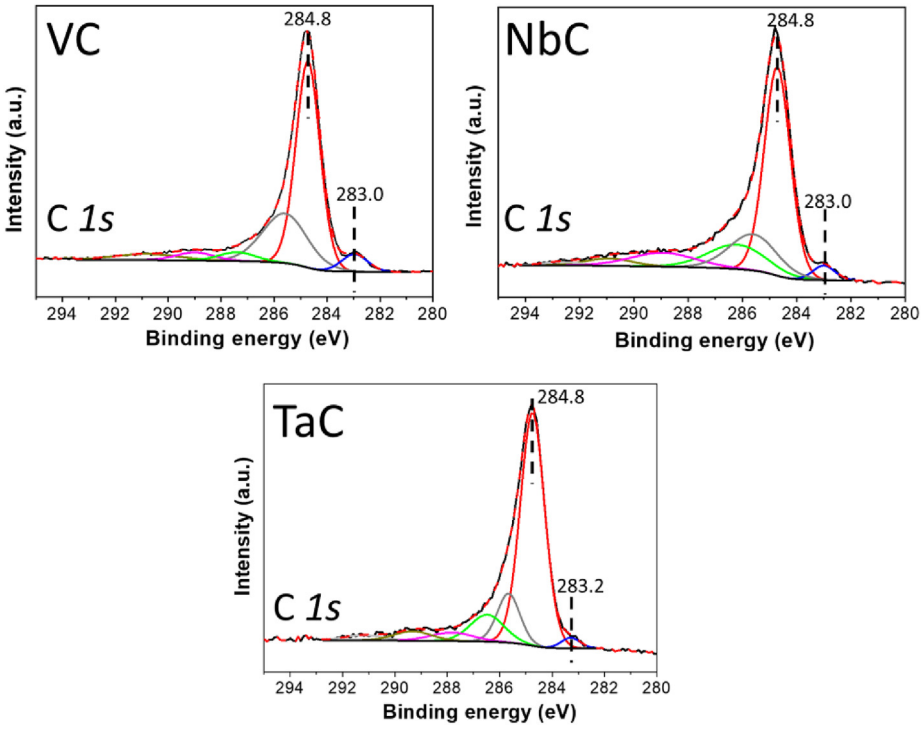

Fig. 7 – XPS profiles of C 1s level of VC, NbC and TaC samples.

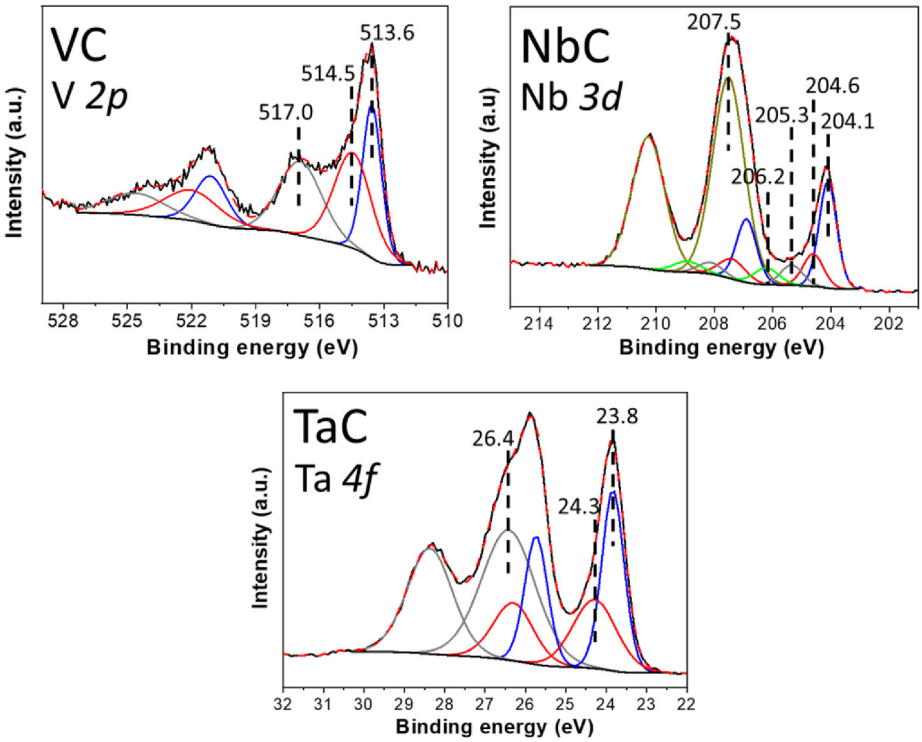

Fig. 8 – XPS spectra of V 2p, Nb 3d and Ta 4f levels of VC, NbC and TaC samples, respectively.

after methanol adsorption at 293 K [40], and over NbC(100) only molecular CH_3OH adsorption has been proposed to take place [40].

The transformation of methanol through the route of dehydrogenation could involve not only the production of HCHO and H_2 (eq. (6)), but also that of CO from HCHO decomposition reaction (eq (7)).

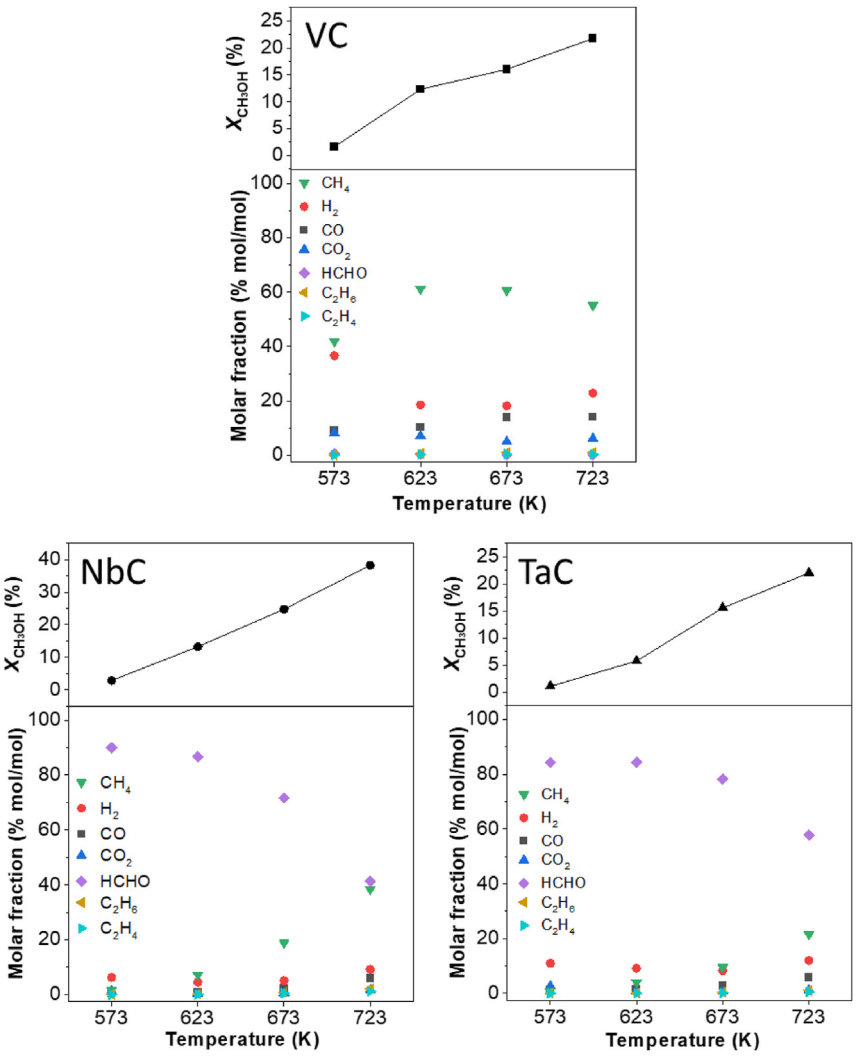

Fig. 9 – Methanol conversion and product distribution (molar fraction) in the MSR reaction over G5TMCs as a function of reaction temperature. Reaction conditions: 300 mg of catalyst, $CH_3OH/H_2O/N_2$ = 1/1/1.2, P = 0.1 MPa and GHSV = 2500 h^{-1}.

$$HCHO_{(g)} \rightarrow CO_{(g)} + H_{2(g)} \quad \text{(eq. 7)}$$

The high $HCHO/H_2$ molar ratio found in the overall temperature range could be related with the consumption of part of H_2 formed in the reduction of surface oxy-carbide species formed under reaction conditions. Moreover, at temperatures higher than 623 K, a similar route to that proposed for VC catalyst, involving CH_3OH decomposition to CH_4, could take place also in some extension over NbC and TaC catalysts.

In order to gain insight into the different transformation routes of methanol over G5TMC catalysts, as described in the experimental section, in separate experiments the effect of the contact time in the 598–623 K range was studied over VC and NbC, which are representative catalysts of the two different patterns of product distribution. Table 2 shows the effect of GHSV variation on methanol conversion and product distribution; the selectivity to C-containing compounds is shown in Table S1. As expected, VC and NbC showed a decrease in methanol conversion when the GHSV was increased from 6000 to 8000 h^{-1}; In all cases, CH_4 and HCHO were the major products for VC and NbC, respectively.

Despite the different MeOH conversion values, in all cases, over VC, CH_4 was produced with a selectivity among C-containing products above 70% (Table S1). For VC, an increase of CH_4 selectivity is observed with the decrease of contact time, pointing out CH_4 as primary product. Over VC, the main reaction pathway seems to be the direct CH_4 formation from C–O scission of CH_3OH (eq. (2)).

For NbC, HCHO selectivity among C-containing products was above 86% (Table S1); over this catalyst, the dehydrogenation of methanol could be proposed as the main reaction pathway (eq. (6)). However, for NbC, when the temperature or GHSV was increased, a slight diminution on HCHO selectivity and a slight increase on CH_4 selectivity were observed. This indicates that, over NbC, CH_4 formation through methanol decomposition might also proceed in some extension. Moreover, for VC and NbC, the $n_{CH_4}/(n_{CO}+n_{CO_2})$ molar ratio decreased when the methanol conversion increased, by varying the GHSV at the same temperature. This point out a

Table 2 – Effect of GHSV on methanol conversion and product distribution for VC and NbC catalysts under MSR. Reaction conditions: 500 mg of catalyst and P = 0.1 MPa.

Catalyst	VC				NbC			
GHSV (h^{-1})	6000		8000		6000		8000	
Temperature (K)	598	623	598	623	598	623	598	623
MeOH Conversion (%)	10.3	21.4	3.6	14.9	5.4	13.6	3.7	10.3
Product Distribution (%)								
H_2	25.3	19.8	22.9	18.7	8.1	5.9	5.9	6.2
CH_4	55.6	59.0	61.7	62.4	5.6	8.1	8.2	10.0
CO_2	7.3	6.4	4.0	5.1	1.0	0.6	0.4	0.5
CO	10.7	13.5	9.7	12.5	0.4	1.6	1.5	1.3
HCHO	0.4	0.2	0.8	0.2	84.7	83.3	83.6	81.4
C_2H_6	0.4	0.7	0.6	0.7	0.1	0.3	0.2	0.3
C_2H_4	0.3	0.4	0.3	0.4	0.1	0.2	0.2	0.3

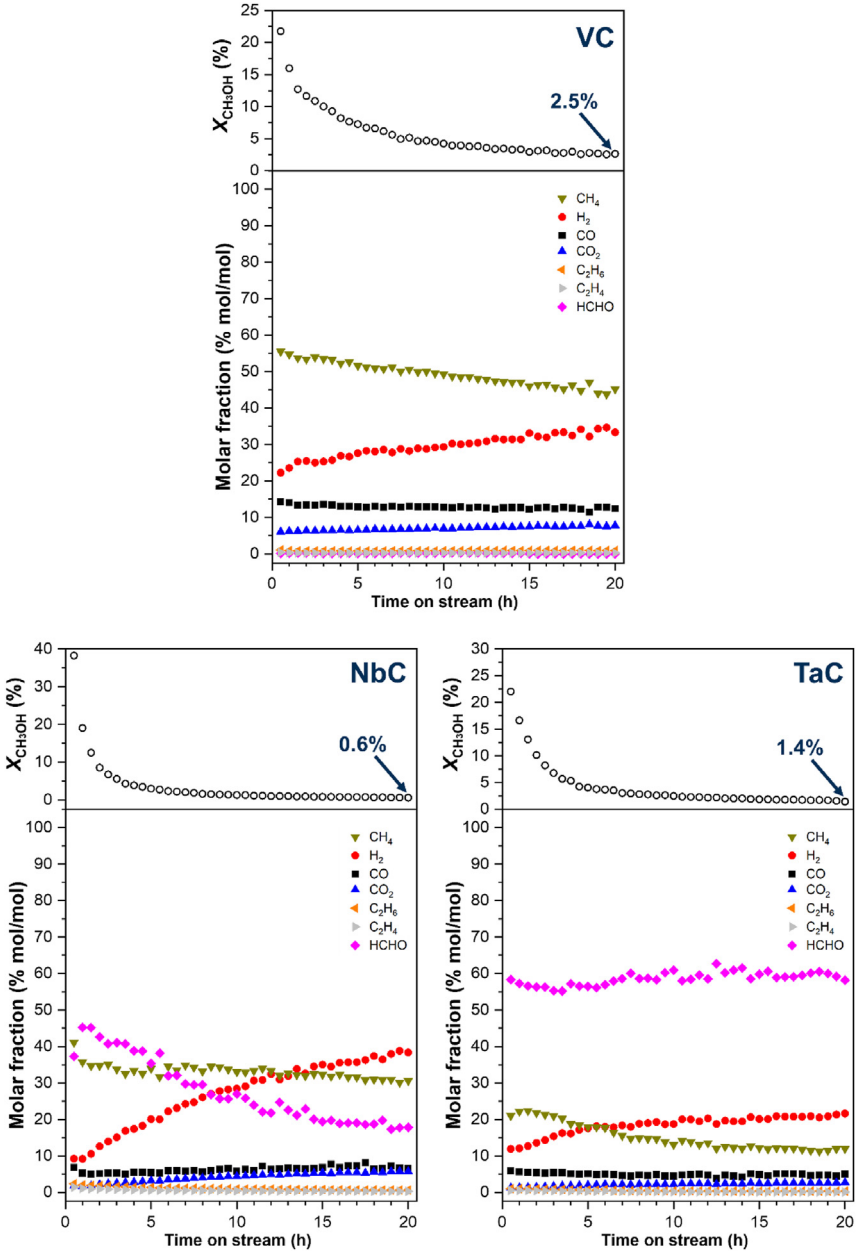

Fig. 10 – Catalytic behaviour of G5TMC in MSR at 723 K along the time, determined after catalytic tests shown in Fig. 9. Reaction conditions: 300 mg of catalyst, $CH_3OH/H_2O/N_2$ = 1/1/1.2, P = 0.1 MPa, GHSV = 2500 h^{-1}.

low contribution, if it exists, of the methanation reactions (eqs. (3) and (4)).

As stated in the experimental section, in the present work, we carried out also a preliminary study regarding the stability of the G5TMC systems under MSR conditions. For such purposes, catalysts were kept at 723 K for 20 h at the final part of the catalytic test. In all cases, a high deactivation was observed. Fig. 10 shows the catalytic behaviour of the catalysts during this period. Except for NbC, only slight variations in the product distribution were observed, in this case a continuous increase of H_2 concentration along time was found.

Post-reaction catalysts were characterized by N_2 adsorption/desorption isotherms, XRD, TGA/DSC analysis and Raman spectroscopy. Despite the large deactivation observed after 20 h at the highest reaction temperature, the crystallite sizes of VC, NbC, and TaC of used catalysts determined from XRD (Fig. S1) resulted equal to those of the corresponding fresh catalysts and, no crystalline metal oxides were observed in any case. However, in all cases, the XRD patterns of the used catalysts showed the presence of a wide peak at $2\theta = 25.0°$ (Fig. S1) and a high decrease of S_{BET} area was observed (Table 1). This could be associated with the presence of carbon deposits formed during the reaction and related with the observed deactivation of catalysts.

Raman spectroscopy is a useful technique for the characterization of the carbonaceous deposits formed in reformation processes [41–44]. In all cases, Raman spectra of post-reaction catalysts revealed intense bands at about 1350 and 1600 cm^{-1} (Fig. 2), indicating the formation of carbonaceous deposits during the long term catalytic test (Fig. 10). After a proper deconvolution of the spectra, the degree of graphitization of the carbonaceous deposits can be estimated by the G/D area ratio [16]. For the used catalysts, an increase in the G/D area ratio is noted when compared to the corresponding values of residual carbon in the fresh catalysts (Table 1). Finally, the used VC was analysed by TGA. Although besides carbon burning, oxidation processes of carbide species could take place, the CO_2 profile can be used in the characterization of deposited carbon (Fig. S2). The formation of abundant carbon deposits during MSR, which are burnt at higher temperature than initial residual carbon in the sample can be noted.

The CH_4 decomposition could lead to coke formation on surface as observed on Mo_2C in the MSR [11,13]. In this context, after methanol adsorption, the decomposition of methanol with carbon formation was also observed on VC(110) single crystals [38]. Moreover, over VC(100) the decomposition of surface methoxy species could form (-CH_xO-), a cyclic intermediate bonded to the surface through both C and O, which has been proposed as precursor of carbonaceous deposits [45]. On the other hand, oxidation and reduction could be in competition under reaction conditions, as has been demonstrated during the methane dry reforming over G5TMC [46]. Despite surface oxidation could contribute to deactivation, as it has been reported for Mo_2C-based catalysts in MSR [15,47], the fact that XRD patterns of used catalysts (Fig. S1) did not show the presence of oxides, could indicate that the deactivation observed could be mainly related with the coke formation. At this respect, to avoid extensive deactivation, different approaches, including the introduction of CO_2 in the reactant mixture, the change of the steam/C ratio, and the use of CO_2 in regeneration processes [48–51], could help to further study G5TMC in the catalytic methanol transformation.

Conclusions

The preparation method used in this work, led to G5TMC (VC, NbC and TaC), with similar crystallite sizes (9–11 nm). G5TMC were active catalysts for the transformation of methanol under MSR stoichiometric reaction conditions ($CH_3OH/H_2O = 1/1$) in the temperature range of 573–723 K. The catalytic behaviour depended on the G5TMC used. VC was active for the selective decomposition of methanol to CH_4, allowing the production of methane-rich (H_2+CH_4) mixtures with $(H_2+CH_4)_{produced}/CH_3OH_{converted}$ up to 0.8 mole ratios. NbC and TaC catalysts exhibited a quite different catalytic behaviour than VC. Over NbC and TaC, the methanol dehydrogenation to formaldehyde is proposed to be the main reaction pathway under the MSR conditions used. At 573 K, the selectivity of HCHO referred to C-containing products is over 95%. All catalysts suffered severe deactivation at the highest temperature (723 K), which is probably related to the formation of carbon deposits under the MSR conditions used. However, in all cases, the crystallite size of the post-reaction G5TMC remained similar to that of the corresponding fresh catalyst and crystalline metal oxides were not detected after reaction.

Declaration of competing interest

The authors declare that they have no known competing financial interests or personal relationships that could have appeared to influence the work reported in this paper.

Acknowledgments

The authors thank MICINN MAT2017-87500-P and PID2020-116031RB I00/AEI/10.13039/501100011033/FEDER projects for financial support. A. P. thanks to MINECO the PhD grant BES-C-2015-074574.

Appendix A. Supplementary data

Supplementary data to this article can be found online at https://doi.org/10.1016/j.ijhydene.2023.06.017.

REFERENCES

[1] Staffell I, Scammman D, Velazquez-Abad A, Balcombe P, Dodds PE, Ekins P, Shah N, Ward KR. The role of hydrogen

and fuel cells in the global energy system. Energy Environ Sci 2019;12:463–91. https://doi.org/10.1039/C8EE01157E.
[2] Patonia A, Poudineh R. Global trade of hydrogen: what is the best way to transfer hydrogen over long distances?. OIES paper ET16 The Oxford Institute for Energy Studies; September 2022. ISBN 978-1-78467-205-8.
[3] Niermann M, Drünert S, Kaltschmitt M, Bonhoff K. Liquid organic hydrogen carriers (LOHCs) – techno-economic analysis of LOHCs in a defined process chain. Energy Environ Sci 2019;12:290–307. https://doi.org/10.1039/C8EE02700E.
[4] Levy RB, Boudart M. Platinum-Like behavior of tungsten carbide in surface catalysis. Science 1973;181:547–9. https://10.1126/science.181.4099.547.
[5] Liu X, Kunkel C, Ramírez De La Piscina P, Homs N, Viñes F, Illas F. Effective and highly selective CO generation from CO_2 Using a polycrystalline α-Mo_2C catalyst. ACS Catal 2017;7:4323–35. https://doi.org/10.1021/acscatal.7b00735.
[6] Pajares A, Prats H, Romero A, Viñes F, Ramirez de la Piscina P, Sayós R, Homs N, Illas F. Critical effect of carbon vacancies on the reverse water gas shift reaction over vanadium carbide catalysts. Appl Catal B Environ 2020;267:118719. https://doi.org/10.1016/j.apcatb.2020.118719.
[7] Pajares A, Wang Y, Kronenberg MJ, Ramírez de la Piscina P, Homs N. Photocatalytic H_2 production from ethanol aqueous solution using TiO_2 with tungsten carbide nanoparticles as co-catalyst. Int J Hydrogen Energy 2020;45:20558–67. https://doi.org/10.1016/j.ijhydene.2020.04.010.
[8] Liu X, Pajares A, Calinao-Matienzo DD, Ramírez de la Piscina P, Homs N. Preparation and characterization of bulk Mo_xC catalysts and their use in the reverse water-gas shift reaction. Catal Today 2020;356:384–9. https://doi.org/10.1016/j.cattod.2019.11.011.
[9] Wang Y, Mino L, Pellegrino F, Homs N, Ramírez de la Piscina P. Engineered Mo_xC/TiO_2 interfaces for efficient noble metal-free photocatalytic hydrogen production. Appl Catal B Environ 2022;318:121783. https://doi.org/10.1016/j.apcatb.2022.121783.
[10] Pajares A, Liu X, Busacker JR, Ramírez de la Piscina P, Homs N. Supported nanostructured Mo_xC materials for the catalytic reduction of CO_2 through the reverse water gas shift reaction. Nanomaterials 2022;12:3165. https://doi.org/10.3390/nano12183165.
[11] Széchenyi A, Solymosi F. Production of hydrogen in the decomposition of ethanol and methanol over unsupported Mo_2C catalysts. J Phys Chem C 2007;111:9509–15. https://doi.org/10.1021/jp072439k.
[12] Setthapun W, Bej SK, Thompson LT. Carbide and nitride supported methanol steam reforming catalysts: parallel synthesis and high throughput screening. Top Catal 2008;49:73–80. https://doi.org/10.1007/s11244-008-9070-7.
[13] Barthos R, Solymosi F. Hydrogen production in the decomposition and steam reforming of methanol on Mo_2C/carbon catalysts. J Catal 2007;249:289–99. https://doi.org/10.1016/j.jcat.2007.05.003.
[14] Lin SSY, Thomson WJ, Hagensen TJ, Ha SY. Steam reforming of methanol using supported Mo_2C catalysts. Appl Catal A-Gen 2007;318:121–7. https://doi.org/10.1016/j.apcata.2006.10.054.
[15] Cao J, Ma Y, Guan G, Hao X, Ma X, Wang Z, Kusakabe K, Abudula A. Reaction intermediate species during the steam reforming of methanol over metal modified molybdenum carbide catalysts. Appl Catal B Environ 2016;189:12–8. https://doi.org/10.1016/j.apcatb.2016.02.021.
[16] Valle B, Castaño P, Olazar M, Bilbao J, Gayubo AG. Deactivating species in the transformation of crude bio-oil with methanol into hydrocarbons on a HZSM-5 catalyst. J Catal 2012;285:304–14. https://doi.org/10.1016/j.jcat.2011.10.004.
[17] Liu G, Zhao Z-J, Wu T, Zeng L, Gong J. Nature of the active sites of VO_x/Al_2O_3 catalysts for propane dehydrogenation. ACS Catal 2016;6:5207–14. https://doi.org/10.1021/acscatal.6b00893.
[18] Bulushev DA, Kiwi-Minsker L, Rainone F, Renken A. Characterization of surface vanadia forms on V/Ti-Oxide catalyst via temperature-programmed reduction in hydrogen and spectroscopic methods. J Catal 2002;205:115–22. https://doi.org/10.1006/jcat.2001.3427.
[19] Hernández-Mejía C, Vogt C, Weckhuysen BM, de Jong KP. Stable niobia-supported nickel catalysts for the hydrogenation of carbon monoxide to hydrocarbons. Catal Today 2020;343:56–62. https://doi.org/10.1016/j.cattod.2018.11.036.
[20] Ding S, Liu F, Shi X, He H. Promotional effect of Nb additive on the activity and hydrothermal stability for the selective catalytic reduction of NO_x with NH_3 over $CeZrO_x$ catalyst. Appl Catal B Environ 2016;180:766–74. https://doi.org/10.1016/j.apcatb.2015.06.055.
[21] Wachs IE, Chen Y, Jehng J-M, Briand LE, Tanaka T. Molecular structure and reactivity of the group V metal oxides. Catal Today 2003;78:13–24. https://doi.org/10.1016/S0920-5861(02)00337-1.
[22] Gupta A, Mittal M, Singh MK, Suib SL, Pandey OP. Low temperature synthesis of NbC/C nano-composites as visible light photoactive catalyst. Sci Rep 2018;8:13597. https://doi.org/10.1038/s41598-018-31989-z.
[23] Alhajri NS, Yoshida H, Anjum DH, Garcia-Esparza AT, Kubota J, Domen K, Takanabe K. Synthesis of tantalum carbide and nitride nanoparticles using a reactive mesoporous template for electrochemical hydrogen evolution. J Mater Chem 2013;1:12606–16. https://doi.org/10.1039/C3TA12984E.
[24] Sonia FJ, Kalifa H, Aslam M, Mukhopadhyay A. Correlations between preparation methods, structural features and electrochemical Li-storage behavior of reduced graphene oxide. Nanoscale 2017;9:11303–17. https://doi.org/10.1039/C7NR03348F.
[25] Enterría M, Martín-Jimeno FJ, Suárez-García F, Paredes JI, Pereira MFR, Martis JI, Martínez-Alonso A, Tascón JMD, Figueiredo JL. Effect of nanostructure on the supercapacitor performance of activated carbon xerogels obtained from hydrothermally carbonized glucose-graphene oxide hybrids. Carbon 2016;105:474–83. https://doi.org/10.1016/j.carbon.2016.04.071.
[26] Zhu Y, Murali S, Stoller MD, Ganesh KJ, Cai W, Ferreira PJ, Pirkle A, Wallace RM, Cychosz KA, Thommes M, Su D, Stach EA, Ruoff RS. Carbon-based supercapacitors produced by activation of graphene. Science 2011;332:1537–41. https://doi.org/10.1126/science.1200770.
[27] Figueiredo JL, Pereira MFR, Freitas MMA, Órfao JJM. Modification of the surface chemistry of activated carbons. Carbon 1999;37:1379–89. https://doi.org/10.1016/S0008-6223(98)00333-9.
[28] Choi J-G. The surface properties of vanadium compounds by X-Ray photoelectron spectroscopy. Appl Surf Sci 1999;148:64–72. https://doi.org/10.1016/S0169-4332(99)00132-4.
[29] Biesinger MC, Lau LWM, Gerson AR, Smart RSC. Resolving surface chemical states in XPS analysis of first row transition metals, oxides and hydroxides: Sc, Ti, V, Cu and Zn. Appl Surf Sci 2010;257:887–98. https://doi.org/10.1016/j.apsusc.2010.07.086.
[30] Su T, Peng R, Hood ZD, Naguib M, Ivanov IN, Keum JK, Qin Z, Guo Z, Wu Z. One-step synthesis of $Nb_2O_5/C/Nb_2C$ (MXene) composites and their use as photocatalysts for hydrogen evolution. ChemSusChem 2018;11:688–99. https://doi.org/10.1002/cssc.201702317.
[31] Simpson R, White RG, Watts JF, Baker MA. XPS investigation of monatomic and cluster argon ion sputtering of tantalum

pentoxide. Appl Surf Sci 2017;405:79–87. https://doi.org/10.1016/j.apsusc.2017.02.006.
[32] Levis RJ, Zhicheng J, Winograd N. Thermal decomposition of CH_3OH adsorbed on Pd{111}: a new reaction pathway involving CH_3 formation. J Am Chem Soc 1989;111:4605–12. https://doi.org/10.1021/ja00195a013.
[33] Solymosi F, Revesz K. Thermal stability of the CH_3 group adsorbed on the Pd(100) surface. J Am Chem Soc 1991;113:9145–7. https://doi.org/10.1021/ja00024a019.
[34] Rebholz M, Kruse N. Mechanisms of methanol decomposition on Pd{111}. J Chem Phys 1991;95:7745–59. https://doi.org/10.1063/1.461348.
[35] Chen J-J, Jiang Z-C, Zhou Y, Chakraborty BR, Winograd N. Spectroscopic studies of methanol decomposition on Pd [1cub]111[rcub]. Surf Sci 1995;328:248–62. https://doi.org/10.1016/0039-6028(95)00007-0.
[36] Morkel M, Kaichev VV, Rupprechter G, Freund H-J, Prosvirin IP, Bukhtiyarov VI. Methanol dehydrogenation and formation of carbonaceous overlayers on Pd(111) studied by high-pressure SFG and XPS spectroscopy. J Phys Chem B 2004;108:12955–61. https://doi.org/10.1021/jp048149a.
[37] Bianchi D, Chafik T, Khalfallah M, Teichner SJ. Intermediate species on zirconia supported methanol aerogel catalysts V. Adsorption of methanol. Appl Catal A-Gen 1995;123:89–110. https://doi.org/10.1016/0926-860X(94)00242-8.
[38] Zellner MB, Hwu HH, Chen JG. Comparative studies of methanol decomposition on carbide-modified V(110) and Ti(0001). Surf Sci 2005;598:185–99. https://doi.org/10.1016/j.susc.2005.09.027.
[39] Frantz P, Didziulis SV, Fernandez-Torres LC, Guenard RL, Perry SS. Reaction of methanol with TiC and VC(100) surfaces. J Phys Chem B 2002;106:6455–64. https://doi.org/10.1021/jp0145311.
[40] Kojima I, Orita M, Miyazaki E. Adsorption of O_2, CO and CH_3OH on NbC(100) and (111) single crystal surfaces by ultraviolet photoelectron spectroscopy. Surf Sci 1985;160:153–63. https://doi.org/10.1016/0039-6028(85)91033-7.
[41] Elias KFM, Bednarczuk L, Assaf EM, Ramírez de la Piscina P, Homs N. Study of Ni/CeO_2–ZnO catalysts in the production of H_2 from acetone steam reforming. Int J Hydrogen Energy 2019;44:12628–35. https://doi.org/10.1016/j.ijhydene.2018.10.191.
[42] Xiu L, Toyir J, Ramírez de la Piscina P, Homs N. Hydrogen production from methanol steam reforming over Al_2O_3- and ZrO_2-modified CuOZnOGa_2O_3 catalysts. Int J Hydrogen Energy 2017;42:13704–11. https://doi.org/10.1016/j.ijhydene.2016.12.133.
[43] Yermán L, Homs N, Pereira EB, Ramírez de la Piscina P. H_2 production from oxidative steam reforming of 1-propanol and propylene glycol over yttria-stabilized supported bimetallic Ni–M (M = Pt, Ru, Ir) catalysts. Int J Hydrogen Energy 2014;39:5225–33. https://doi.org/10.1016/j.ijhydene.2013.12.163.
[44] Cai W, Ramírez de la Piscina P, Homs N. Oxidative steam reforming of bio-butanol for hydrogen production: effects of noble metals on bimetallic CoM/ZnO catalysts (M = Ru, Rh, Ir, Pd). Appl Catal B Environ 2014;145:56–62. https://doi.org/10.1016/j.apcatb.2013.03.016.
[45] Frantz P, Kim HI, Didziulis SV, Li S, Chen Z, Parry SS. Reaction of methyl formate with VC(100) and TiC(100) surfaces. Surf Sci 2005;596:144–62. https://doi.org/10.1016/j.susc.2005.09.010.
[46] Brungs A, York APE, Green MLH. Comparison of the group V and VI transition metal carbides for methane dry reforming and thermodynamic prediction of their relative stabilities. Catal Lett 1999;57:65–9. https://doi.org/10.1023/A:1019062608228.
[47] Ma Y, Guan G, Shi G, Zhu A, Hao X, Wang Z, Kusakabe K, Abudula A. Low-temperature steam reforming of methanol to produce hydrogen over various metal-doped molybdenum carbide catalysts. Int J Hydrogen Energy 2014;39:258–66. https://doi.org/10.1016/j.ijhydene.2013.09.150.
[48] de Lima SM, da Silva AM, Jacobs G, Davis BH, Mattos LV, Noronha FB. New approaches to improving catalyst stability over Pt/ceria during ethanol steam reforming: Sn addition and CO_2 co-feeding. Appl Catal B Environ 2010;96:387–98. https://doi.org/10.1016/j.apcatb.2010.02.036.
[49] Bespalko N, Roger A-C, Bussi J. Comparative study of NiLaZr and CoLaZr catalysts for hydrogen production by ethanol steam reforming: effect of CO_2 injection to the gas reactants. Evidence of Rh role as a promoter. Appl Catal A-Gen 2011;407:204–10. https://doi.org/10.1016/j.apcata.2011.08.042.
[50] Bednarczuk L, Ramírez de la Piscina P, Homs N. H_2-production from CO_2-assisted ethanol steam reforming: the regeneration of Ni-based catalysts. Int J Hydrogen Energy 2015;40:5256–63. https://doi.org/10.1016/j.ijhydene.2015.01.061.
[51] Bednarczuk L, Ramírez de la Piscina P, Homs N. Efficient CO_2-regeneration of Ni/Y_2O_3-La_2O_3-ZrO_2 systems used in the ethanol steam reforming for hydrogen production. Int J Hydrogen Energy 2016;41:19509–17. https://doi.org/10.1016/j.ijhydene.2016.05.038.